Optics Letters

Compact self-illuminated image upconversion system based on intracavity second-harmonic generation

A. J. Torregrosa,[1] H. Maestre,[1] M. L. Rico,[2] and J. Capmany[1,*]

[1]Communications Engineering Department, Universidad Miguel Hernández, Avda. de la Universidad s/n, 03202 Elche, Spain
[2]Computer Science Department, Universidad de Alicante, Ctra. San Vicente s/n, 03690 San Vicente del Raspeig, Spain
*Corresponding author: jcapmany@umh.es

Received 9 August 2018; revised 11 September 2018; accepted 14 September 2018; posted 14 September 2018 (Doc. ID 341841); published 10 October 2018

We present an image upconversion system based on intracavity Type II second-harmonic generation to create an image in the visible spectrum of a target illuminated by an infrared laser. The system has the novelty of being self-illuminated. It uses some fractional leaking power of the infrared laser to illuminate a target located in the object focal plane of the system, and to couple back a created infrared target image to an intracavity nonlinear crystal, where it mixes with the cavity laser beam to obtain a second-harmonic image, visible with a silicon CCD camera. For a proof of concept, we have built a system based on a diode-pumped Nd^{3+}:YVO_4 continuous-wave (cw) laser and an intracavity KTP crystal to upconvert 1342 nm target images to 671 nm. The upconverted cw power allowed us to capture real-time video in a standard nonintensified CCD camera, with 2.5 W of a diode pump.

OCIS codes: (190.4223) Nonlinear wave mixing; (110.3080) Infrared imaging; (140.3613) Lasers, upconversion; (140.3580) Lasers, solid-state.

https://doi.org/10.1364/OL.43.005050

Nonlinear image upconversion is a useful technique to visualize infrared (IR) images with standard silicon CCD or CMOS cameras. First proposed and demonstrated back in the late 1960s by Midwinter [1], this field remained almost unexplored until 2009, when Pedersen *et al.* [2] reported an intracavity continuous-wave (cw) image upconversion system based on a PPKTP crystal placed inside a Nd^{3+}:YVO_4 laser cavity. Since then, this field is regaining research attention, and rapid progress is being made based on intracavity upconversion [3,4].

Despite other potential applications of image upconversion, it has been reported that illumination of some biological tissues/cells in the near or short-wave infrared (NIR, SWIR) is noninvasive and nondestructive for *in vivo* observation [5].

Most frequently, nonlinear image upconversion is done through a sum-frequency mixing (SFM) interaction based on the $\chi^{(2)}$ nonlinear susceptibility, although image upconversion based on other nonlinear processes such as four-wave mixing and second-harmonic generation (SHG) has been reported [6,7]. In general, the original IR image of an emitting or laser-illuminated target gets mixed with an intense auxiliary laser (pump laser) to provide simultaneous optical heterodyning of the 2D Fourier components of the IR image in a nonlinear crystal. Thus, image upconversion requires noncollinear nonlinear interactions taking place simultaneously. For the best resolution, a Gaussian pump laser beam should be used [2].

In particular, the only report so far to our knowledge based on degenerate (harmonic) optical heterodyning is by use of a resonant external enhancing SHG self-imaging linear cavity, leading to a limited image resolution due to severe cavity spatial filtering, that makes it difficult to produce SHG of complex images [7]. The self-imaging cavity requires active length stabilization, and it is not assisted by an intense auxiliary intracavity pump beam to enhance conversion efficiency.

Here, we explore the feasibility of a system architecture for cw intracavity-laser-assisted upconversion to the second harmonic (SH) of an IR-illuminated target located at the input focal plane of the whole upconverting optical system. The system has the novelty of being self-illuminated, i.e., of employing part of the pump laser power to illuminate the target, thus avoiding the necessity of an auxiliary laser as in SFM. In this way, the kind of system discussed here can be made very compact, so that it could set the basis for future practical portable or even handheld systems, which would only require to position the system relative to a sample, so that its input focal plane matches the location of a target or sample to be IR illuminated and imaged in the visible.

Such a self-illuminated system needs first to extract some power from the intracavity pump laser for target illumination. Second, it needs to provide a mechanism for coupling and extracting the IR and upconverted images in and out of the cavity, and finally, it needs to prevent the pump laser mode from producing intracavity SHG itself in the absence of an IR target image. For this purpose, we describe a system architecture based on the combined use of a polarizing beam splitter (PBS) and Type II birefringent phase matching (BPM). Usually, image coupling and extraction in image upconversion systems are realized

with wavelength-dependent dichroic beam splitters [2–4]. However, this resource is not possible in SHG, where the pump laser and the IR image share the same wavelength. The basic system architecture used is represented in Fig. 1(a). The IR laser oscillates in a linear polarization perpendicular to the paper. The PBS outcouples a small fraction of the intracavity power to illuminate a target. An IR target image in the crossed polarization is then created and sent to the cavity, entering the cavity with a negligible loss, where it mixes with the intracavity laser beam in the nonlinear crystal in a single-pass Type II SHG process [Fig. 1(b)]. In the most integrated version, a dielectric high reflection (HR) output coupler can be coated on the nonlinear crystal, all the components can be glued or bonded together, and the pump diode can be brought in close proximity to the laser crystal with no focusing optics.

For a proof of concept, we built the system described in Fig. 2(a). The pump laser cavity is an L-folded cavity composed by the HR output coupler (nominal $R = 99.7\%$ only at ~1342 nm to avoid oscillation at 1064 nm), the flat folding surface inside the PBS ($5 \times 5 \times 5$ mm^3), and a standard commercial HR dielectric mirror of unknown reflectivity (typically $R \geq 99.5\%$) deposited on the laser crystal, with high transmission for the diode pump. The folding surface has a high nominal reflectivity for the polarization perpendicular to the figure ($T_s = 0.16\%$), and a high nominal transmission for the in-plane polarization ($T_p = 97.86\%$). The laser crystal is a flat–flat

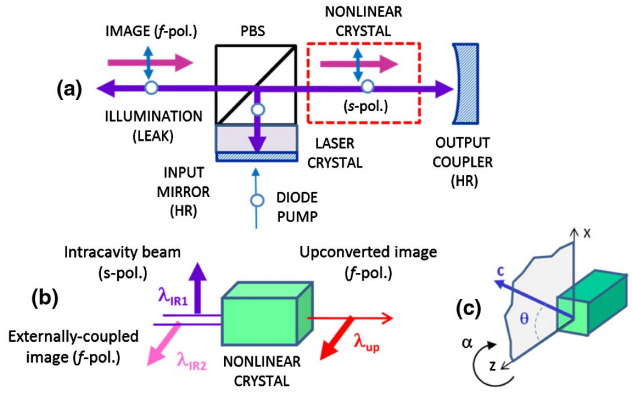

Fig. 1. Schematic diagram of the experimental setup used for self-illuminated image upconversion.

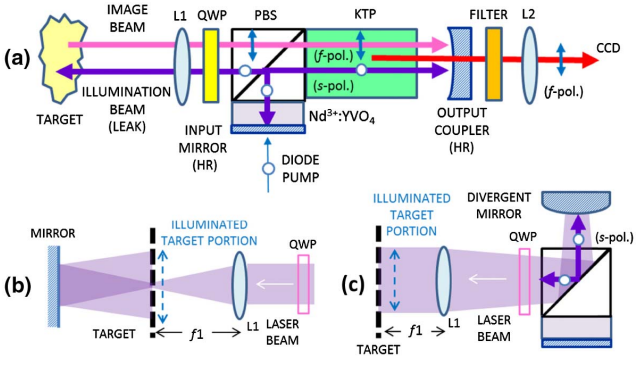

Fig. 2. (a) Schematic diagram of the complete experimental setup used for self-illuminated image upconversion. Illumination expansion for (b) transmission and (c) reflection modes.

5-mm-long 3 mm × 3 mm a-cut 1% at. doped Nd^{3+}:YVO_4, with antireflection (AR) coating on the internal cavity side. The crystal *a*-cut orientation favors a linearly polarized oscillation perpendicular to the figure. The crystal was wrapped around with an indium foil, and attached to a small copper heat-sink holder. Under focused diode end-pumping at 808 nm, it oscillates at 1342 nm in the $^4F_{3/2} \rightarrow {}^4I_{13/2}$ luminescent channel of Nd^{3+}, with a linear polarization vertical to the figure, and in a fundamental Gaussian mode of 350 μm measured beam radius that remains essentially constant along the cavity and the KTP crystal, and within the distances involved in our imaging system (≈0.5 m Rayleigh range).

A low-pass filter ($\lambda < 700$ nm) was placed behind the output coupler to block the remaining fundamental and diode pump.

The pump collimation and focusing is done with a demagnifying 2:1 telescope consisting of two aspheric lenses of short focal length (1–2 mm) in close proximity. The laser crystal is in physical contact with the PBS, and the almost flat output coupler (concave, 3 m radius of curvature) is located 5 cm away from the PBS. We left such a distance between the output coupler and the PBS in order to easily allocate a nonlinear KTP crystal in a three-axis rotational orientation crystal holder for phase matching (PM) optimization. This distance can be shortened in a practical system down to the KTP length by removing the KTP holder, and bringing all the components to physical contact in a most compact configuration of around 2 cm × 2 cm × 0.6 cm volume, excluding the pump diode and the imaging system to be discussed later. In our experiments, the lengths of the folded cavity arms are then around 1 and 5 cm.

The KTP crystal is an 8-mm-long 6 mm × 6 mm flat–flat bulk crystal, cut at $\theta = 60°$, $\varphi = 0°$ for critical Type II SHG of 1342–671 nm, with its fast (ordinary) and slow (extraordinary) axis coincident with the crystal lateral facets. The crystal cavity facets are both AR-coated for the 1342 and 671 nm wavelengths, and the nonlinear effective coefficient is around 3 pm/V. This is a low nonlinear coefficient as compared with Type 0 quasi-phase matching (QPM) in poled ferroelectric crystals, with typical nonlinear effective coefficients in the range 8–18 pm/V. This is the price paid for the other benefits of the compact architecture of the system, not realizable with Type 0 QPM, and particularly its potential increased resolution, as discussed later. However, the potential for high intracavity SHG efficiency even with nonlinear coefficients lower than those typical of Type 0 QPM is well known after the work by Smith [8], and it is well supported by the widespread Nd^{3+}:YVO_4+ KTP glued green microchip lasers, typical of green laser pointers based on Type II intracavity SHG.

A birefringent intracavity crystal oriented at an arbitrary α-angle around the *z* axis in Fig. 1(c), with respect to the empty cavity laser polarization axis, introduces in general some orthogonal polarization, and leads therefore to SHG of the laser mode itself, that we will call parasite SHG in what follows. The analysis of the cavity polarization eigenstates with two birefringent intracavity crystals (*a*-cut YVO_4 and KTP in our case) and intracavity polarization elements as the PBS is complex, and can be examined in Refs. [9,10]. For this reason, rather than the usual $\alpha = 45°$ for optimal intracavity SHG of a laser beam, the Type II crystal must be aligned with one of its fast or slow axes parallel to the empty cavity polarization axis (the slow axis $\alpha = 0°$ in our case). As a result, the leaking illumination would be of the same polarization as the laser, giving no option to

SHG of the IR target image, as some fast polarization component is required for the Type II BPM. For these reasons, the architecture here discussed must be discarded in case of Type I BPM or Type 0 QPM. Further, the low transmission for the slow polarization in the PBS would prevent the IR image from re-entering the cavity. The folding surface introduces a high cavity loss for any hypothetical oscillation in the horizontal polarization. Due to the KTP orientation in our cavity relative to the spectroscopic π polarization of the a-cut Nd^{3+}:YVO_4 crystal, the laser oscillates in only one polarization eigenstate corresponding to the slow axis of the KTP crystal, as checked with a polarizer.

Without the KTP crystal, the laser oscillates in linear polarization perpendicular to the paper in Fig. 1(a), with an estimated intracavity power of around 10 W, and with a measured power of 16 mW leaking through the PBS towards the target for a diode pump power of 2.5 W. When the KTP crystal is introduced inside the cavity, the estimated intracavity power reduces to ~2/3 for the same diode pump power (10.6 mW of vertical polarization output). With no fine adjustment of the KTP orientation, a central intense spot of parasite SHG can be seen in the CCD camera even in the absence of an IR target image. As expected, the intensity of the parasite SHG spot is affected by the α-angle orientation; so careful and patient adjustment is needed to remove it, as discussed below. Indeed, the s- and f-polarization components ratio at 1342 nm measured at the illumination output, and therefore the present intracavity, are very sensitive to the KTP α-angle crystal orientation.

Figures 3(a)–3(h) show the relative spectral powers measured in both polarizations in the direction towards the target. As the α-angle is rotated from 0 to 2 deg away from the condition $\alpha = 0°$, a leaking power is generated in f polarization that increases from 0 up to 12 mW. This radiation serves to illuminate the target creating a SHG image visible in a CCD sensor located

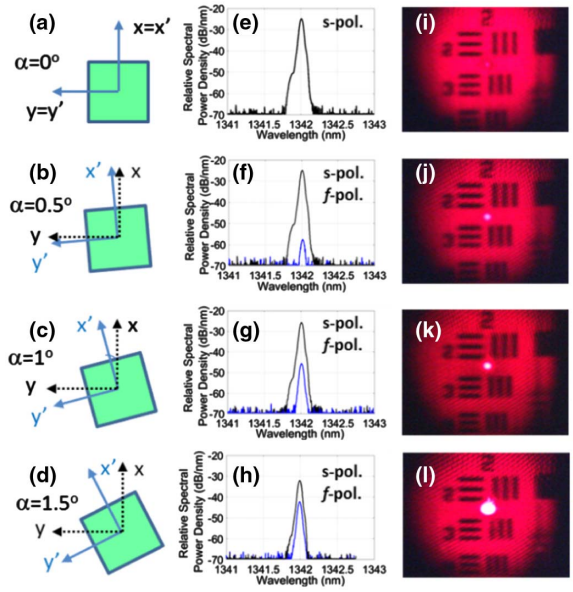

Fig. 3. Upconverted images live-captured from the CCD camera, and relative s- and f-polarization spectral components exiting the PBS towards the target for slight rotations of the KTP crystal around its longitudinal axis. (a), (b), (c), and (d), correspond to $\alpha = 0°$, $\alpha = 0.5°$, $\alpha = 1°$, and $\alpha = 1.5°$, respectively.

at the image focal plane of L2. However, it leads to parasite SHG. This leaking power level is in good agreement with the estimated intracavity power available and the transmission of the PBS in the f polarization. For a 2 deg rotation, the leaking f-polarization component resulting from the birefringence seen by the intracavity beam becomes a projection factor $\sin^2(2°) \approx 1.2 \times 10^{-3}$ of the available intracavity power initially available in the slow polarization for $\alpha = 0°$ ($T_p \approx 0.98$, 10.6 W) i.e., ≈12.4 mW. This represents an additional cavity loss comparable to the $T_s = 0.16\%$ of the PBS for the s polarization, and is to be preferably avoided in the laser. For a 1 deg rotation, however, $\sin^2(1°) \approx 3 \times 10^{-4}$, and only an additional intracavity power loss factor of 0.25 times that of the unavoidable T_s of the PBS for the s polarization results. Thus, although $\alpha \neq 0°$ provides f-polarized target illumination and leads indeed to SH target image formation, it introduces a loss in the laser that reduces intracavity power and produces a parasite SH spot in the center of the SHG image [Figs. 3(i)–3(l)]. Therefore, the best performance requires the KTP be oriented so that the intracavity laser beam sees no effective birefringence, i.e., so that the laser is linearly polarized along a principal axis of the KTP crystal, i.e., when $\alpha = 0°$.

In order to generate f polarization to illuminate the target and to remove parasite SHG with $\alpha = 0°$, a quarter-wave plate (QWP) for the fundamental wave at 1342 nm, rotated 45° with respect to the polarization of the fundamental, is placed between the lens (L1) and the PBS. This leads to circular polarization for target illumination, with around 5.3 mW in f polarization to illuminate the target, and to generate an image sent back to the KTP and upconverted. In this case, the PBS presents high transmission for coupling the f-polarized IR image back into the cavity. The complete system scheme including the image-forming optics is shown in Fig. 2(a).

Because the target illumination beam is a collimated beam that traverses L1 towards the target, the illuminated target area at the input focal plane of L1 is only a small focused spot. A solution is to work in target transmission mode using a mirror as in Fig. 2(b). However, it is more practical to take advantage of the otherwise wasted s-polarized power leaking through the PBS on the facet opposite to the laser crystal as shown in Fig. 2(c). A divergent spherical mirror of small curvature (2–3 cm radius) can be used for expanding illumination on the target via reflection in the PBS to operate in target reflection mode. Thus, the system can operate in either reflection or transmission mode.

The upconverted optical image formation is based on a 4-f Fourier processor system, composed of lenses L1 and L2 of focal lengths $f_1 = 5$ cm and $f_2 = 15$ cm in a telescope configuration. The center of the KTP crystal is located in the Fourier plane, i.e., in the focal plane of L1. The CCD sensor is placed at the image focal point of L2. This configuration is described in more detail in Ref. [2]. It is well known that this configuration results in an upconverted/image size ratio ≈ $(f_1/f_2) \times (\lambda/2\lambda) = f_1/(2f_2)$ [4]. Regarding resolution, the point spread function (PSF) is limited by the laser mode size and the focal length of L1, with the laser Gaussian mode acting as a soft amplitude aperture in the Fourier plane. For this spatially coherent illumination, the shape of the intensity PSF can be well approximated by $\mathrm{PSF}(r) \propto \exp -\{2r/f_1\}^2$, with ω being the laser beam radius, r the distance from the cavity axis, and λ the fundamental wavelength [2]. With our 350 μm laser radius, and $f_1 = 50$ mm, this gives a Gaussian PSF (FWHM) of 50.8 μm, with a 3% modulation transfer function (MTF)

resolution limit of 19.7 line pairs/mm (lp/mm) in the object focal plane of L1 (group 4, element 1 in a 1951 USAF target).

As seen in the PSF, the radius at $1/e^2$ reduces, and therefore resolution in lp/mm increases linearly with the beam radius ω and with $1/f_1$. For this reason, compact systems where the distance between L1 and the KTP crystal can be made short, leading to higher potential resolution. Increasing the beam radius leads also to improved resolution, although at the expense of a lower laser power density in the KTP crystal, which can be compensated for by increasing the diode pump level. For instance, a reduction in f_1 close to $f_1 = 15$ mm, compatible with our compact architecture, would increase resolution to 78.8 lp/mm for the same beam size (group 6, element 2), with a PSF (FWHM) of 12.7 μm. We have not pursued such a short focal length at this stage, due to mechanical limitations in our setup. However, the system architecture would allow for it, as the total length of half the KTP crystal (Fourier plane) plus the PBS thickness is around 9 mm.

Concerning the beam size, intracavity conversion based on QPM with electric-field poled (EFP) crystals is limited to cavity Gaussian mode radii around 300 μm, at least in one transversal direction [3], due to the typical EFP crystal apertures of thickness $A = 1$ mm. This follows from the condition $A \geq 1/(2\omega \times 1.5)$, a requisite for not introducing significant aperture intracavity loss (<1%) in the laser Gaussian mode, a loss that is in strong detriment to intracavity SHG efficiency [8]. With bulk nonlinear crystals, this limitation is removed in the benefit of a potential increase in resolution achievable by enlarging the soft aperture diameter. Another aspect related to resolution is that resolution improves as the IR image field of view (FOV) that is upconverted increases, according to the relation $\sin\theta = \lambda\nu$, where θ and λ are the upconverted angle and wavelength of the IR image, and ν is the spatial frequency associated to a Fourier component in a 2D image [11]. The upconverted FOV is ultimately limited by noncollinear PM angle tolerances that typically remain within the paraxial condition. In this sense, Type II PM can sometimes exploit significantly increased angle tolerances with respect to Type 0 QPM by use of tangential PM, as shown by Warner [12]. Broadening of the BPM- or QPM-matching angle tolerances by creating a thermal gradient in the nonlinear crystal is another resource that can be exploited to increase the FOV [13]. Our preliminary FOV is ~6.8° (full cone angle), with an illuminated target circle of ~6 mm in diameter.

The upconverted images captured in a color CCD camera taken with the system at different α angles in transmission mode with the QWP inserted can be seen in Figs. 3(i)–3(l). Some fringes can be appreciated in the images, presumably related to interference caused in a flat–flat element with imperfect AR coating such as the PBS, the filter, or the KTP crystal.

Yet another characteristic of this system architecture is that the mixing laser may be made to operate in passive Q-switch mode by introducing a saturable absorber crystal between the laser crystal and the PBS, a path not travelled through by the image, due to the cavity L-folding. With typical 10 ns pulse widths, the associated pulse length of the pump and illumination beams is of order 3 m. Due to the short lengths of the system, this gives a good temporal overlap between the pump and image beams to make a synchronized pulsed upconversion [14] that requires no relative delay control, and that would benefit from higher peak power levels to improve conversion efficiency. Although we do not take special advantage of it at present, the fact that the illumination beam and the mixing beam bear a defined phase relation adds a potential resource to exploit temporal coherence in the system. This is not the case when the auxiliary pump laser is uncorrelated in phase with the illumination laser as in SFM.

In summary, we report proof-of-principle results on a feasible and compact system architecture for upconversion by SHG of IR-illuminated targets that can benefit from an intense intracavity beam, and where no additional illumination sources are required. There is clear room for improvement of our preliminary experimental performance, both in resolution and image to SH photon upconversion efficiency (an estimated Quantum Efficiency $\sim 4 \times 10^{-4}$) with well-known standard resources to enlarge the laser mode radius, and to increase the diode pump level. However, in spite of the low conversion efficiency in our system, the cw SH images can be visualized in real time in a standard (nonintensified) CCD color camera operating at a video rate of 30 frames per second (fps), by pumping with a small diode laser at 2.5 W. This PBS-Type II PM architecture has several potential attractive features to be explored and exploited in the future, and can be adapted to other spectral regions in the IR by a suitable choice of the laser/nonlinear crystal combination. Besides the wavelengths available with typical laser crystals, in applications that may require another specific IR wavelength, diode-pumpable laser crystals used for tunable lasers like those based on Cr^{2+}, Cr^{4+}, or Co^{2+} give access to almost all the IR between 1.2 and 3.4 μm [15], leaving the specific IR wavelength choice to a narrowband spectral reflectivity of the cavity mirrors. However, in combination with silicon or InGaAs CCD cameras, the fundamental IR wavelength cannot exceed around 3.4 μm.

Funding. Gobierno de España, Ministerio de Economía y Competitividad (MINECO) (TEC2014-60084-R, TEC2017-88899-C2-1-R); European Regional Development Fund (ERDF).

REFERENCES

1. J. E. Midwinter, IEEE J. Quantum Electron. **4**, 716 (1968).
2. C. Pedersen, E. Karamehmedović, J. S. Dam, and P. Tidemand-Lichtenberg, Opt. Express **17**, 20885 (2009).
3. J. S. Dam, C. Pedersen, and P. Tidemand-Lichtenberg, Opt. Lett. **35**, 3796 (2010).
4. A. J. Torregrosa, H. Maestre, and J. Capmany, Opt. Lett. **40**, 5315 (2015).
5. R. Aviles-Espinosa, S. I. Santos, A. Brodschelm, W. G. Kaenders, C. Alonso-Ortega, D. Artigas-García, and P. Loza-Alvarez, J. Biomed. Opt. **15**, 046020 (2010).
6. O. Ormachea, O. G. Romanov, A. L. Tolstik, J. L. Arce-Diego, F. Fanjul-Velez, and D. Pereda-Cubian, Opt. Express **14**, 8298 (2006).
7. B. Chalopin, A. Chiummo, C. Fabre, A. Maître, and N. Treps, Opt. Express **18**, 8033 (2010).
8. R. G. Smith, IEEE J. Quantum Electron. **6**, 215 (1970).
9. L. Friob, P. Mandel, and E. A. Victorov, Quantum Semiclass. Opt. **10**, 1 (1998).
10. L. Lefort and A. Barthelemy, Opt. Lett. **20**, 1749 (1995).
11. J. W. Goodman, *Introduction to Fourier Optics*, 3rd ed. (Roberts and Company, 2005).
12. J. Warner, Opto-Electronics **1**, 25 (1969).
13. H. Maestre, A. J. Torregrosa, C. R. Fernández-Pousa, and J. Capmany, Opt. Express **26**, 1133 (2018).
14. K. Huang, X. Gu, H. Pan, E. Wu, and H. Zeng, Appl. Phys. Lett. **100**, 151102 (2012).
15. P. M. W. French, Laser Focus World **31**, 93 (1995).